



Quantification of water in hydrophobic and hydrophilic flow channels subjected to gas purging via neutron imaging

Hong-Yue Tang^a, Anthony Santamaria^a, Jae Wan Park^{a,*}, Changwoo Lee^b, Woonbong Hwang^b

^a Department of Mechanical and Aerospace Engineering, University of California, Davis, CA, 95616, United States

^b Department of Mechanical Engineering, Pohang University of Science and Technology, Pohang, Republic of Korea

ARTICLE INFO

Article history:

Received 8 March 2011

Received in revised form 19 May 2011

Accepted 21 May 2011

Available online 30 May 2011

Keywords:

PEM

Fuel cell

Hydrophobicity

Water removal

Purging

ABSTRACT

Water removal from an idle fuel cell is an important issue for start-up/shutdown down under cold temperature conditions. In our study, we performed an in-situ neutron imaging for a PEM fuel cell with bipolar plates, treated with a super-hydrophobic and super-hydrophilic coating on the flow channels. The coatings were applied to the channels but not on the landings in contact with the GDL. The cells were run at a constant voltage prior to shutdown, then sets of neutron images were taken with purge velocities varied from 1 m s^{-1} to 4 m s^{-1} , in intervals of 1 m s^{-1} . It was found that changing the wettability of the flow channels can improve the dynamics of water removal during purging. The super-hydrophilic and super-hydrophobic coating had better performance in removing water on the landings and in the channels, respectively. Based on our test cells, we used the amount of water remaining as a metric and found no significant improvement by purging the cell at velocities greater than 3 m s^{-1} .

© 2011 Elsevier B.V. All rights reserved.

1. Introduction

In an effort to diversify sources of electrical energy, polymer electrolyte membrane (PEM) fuel cells have many potential uses in mobile and stationary applications. Concern about carbon footprint and improving efficiency, makes PEM fuel cells an attractive candidate because they convert fuel into electrochemical power while only releasing water as a byproduct, they also can be integrated into a combined-heat-and-power systems. With the option of using renewable and or bio-derived fuel sources, pollution associated with such fuels can be shifted from point-of-use to the production site. The forthcoming PEM fuel cell applications are in automotive and propulsion applications or emergency power generation [1]. Still, there are a number of barriers, such as the reliability, cost, infrastructure, performance, and system complexity that need to be improved to enable the wide scale adoption of this technology.

Among the technological barriers, water management is one key to improve the performance and reliability of a PEM fuel cell. A balance between too little water and too much must be constantly maintained. The ionic conductivity, a primary driver of performance, of the PEM fuel cell is dependent on the membrane hydration. Excessively low membrane hydration can result in high electrical resistance, leading to dry regions and premature membrane failure, which can reduce reliability. Conversely, exces-

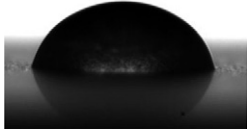


sively high membrane hydration may result in the condensation and flooding of the porous gas diffusion layer (GDL), leading to gas blockages. Fuel may be prevented from reaching reaction sites, causing instability in cell performance. Furthermore, the issue has other implications for fuel cell operation temperature ranges and the start-up/shutdown process [2–5].

Literature points to several approaches specific to water management. These methods fall under the categories of either active or passive methods. Examples of passive methods are the following; using a pressure gradient to drive water from the cathode through the permeable PEM to the anode [6,7–9], MEA designed with a wicking layer [4,10,11], flow field designed using hydraulic resistance to drive out excess liquid water [12,13], creating a hydrophobic and micro-structured flow field [14–16]. Passive methods make use of inherent design features to rid the flow field of excess water. Active methods include electro-osmotic pumping [6], active acoustic wave purging [17,18], periodic flushing or purging [13,19,20], and adjusting pressure between a flow channel and an adjacent channel [21]. These are active methods since they usually require auxiliary equipment and/or power. At high current density operation, a delicate balance of MEA humidification and byproduct removal must be maintained to prevent flooding which is detrimental to cell stability and performance.

The impact of flow channel wettability on fuel cell performance has also been studied [22,23]. Wettability refers to the contact angle of a water droplet on a surface. Generally, if the contact angle is greater than or equal to 90° it is referred to as a hydrophobic surface. Conversely, if the contact angle is less than 90° is referred to

* Corresponding author. Tel.: +1 530 752 5559; fax: +1 530 752 4158.
E-mail address: jwpark@ucdavis.edu (J.W. Park).

Table 1
Surface wettability with various surface treatment technique.

Wetting property	Hydrophilic	Super-hydrophilic	Super-hydrophobic
Process	Sanding	Sand blasting + anodizing	Sand blasting + anodizing + HDFS coating
Contact angle	72.2°	13.5°	152.5°
Image			

as a hydrophilic surface. There are also techniques to create super-hydrophobic and super-hydrophilic surfaces with contact angle over 150° and below 30°, respectively [22,23]. Table 1 shows some examples of the capabilities of our surface treatment techniques. Owejan et al. [3,24] have experimented with both hydrophobic and hydrophilic flow channels. It was found that while the hydrophobic coating retains water in the landing area, the coating allows water to “bead-up” into smaller droplets. These smaller droplets are easier to remove from the flow channel which improves high current density performance. Another study by Yang et al. [25], showed that hydrophilic flow channels enable water extraction from the GDL. The water coating the wall was driven out by the gas flow. Long term degradation needs to be studied as these coatings may suffer degradation from PEM fuel cell thermal cycling and freeze–thaw cycles which may cause thermal–mechanical stress in the coating material.

This paper examines another aspect of the benefits wettability has on flow channels. In the start-up/shutdown of PEM fuel cells in sub-zero temperature environments, the condensation in the flow channels and in the GDL can degrade the life and performance of the cell. Any remaining water in the fuel cell after shutdown may undergo significant volume change due to temperature, which can change the hydrophobicity, electrical resistivity, permeability, porosity, and other properties in the GDL, as well as the ionic conductivity, gas impermeability, and mechanical strength of the membrane [5,26–28]. Thus, water removal prior to shutdown can potentially improve the robustness and reliability of the PEM fuel cell. There have been different visualization works [29–35] and in situ experiments with neutron imaging [3,36,37] to study water droplets behavior in flow channels, as well as numerical studies [38,39] and visualization work [23,38,40,41] on hydrophobic/hydrophilic-coated flow channels. In our study, we performed in situ experiments on two sets of parallel flow channels coated with a super-hydrophobic and super-hydrophilic layer, while imaging the fuel cell with a neutron beam. While this work serves as another verification of similar work, it is also an intermediate step for developing the technique to study water distribution and migration in low temperature operation and cold start. Neutron imaging is a powerful non-destructive testing tool that has shown to be useful in studying in situ fuel cell operations [42]. Fig. 1 shows the schematic of our test setup. With the quasi-real time images of the cell running at various operating point, it is possible to see the distribution and the rate of water production, as well as water redistribution during the start-up/shutdown process.

In this study, in situ experiments were performed on super-hydrophilic and super-hydrophobic flow channels. Two fuel cells were assembled, one using a set of non-coated/super-hydrophilic flow channels and one using a set of non-coated/super-hydrophobic flow channels. A series of neutron images were taken at different stages during the purging of the fuel cell. The results are presented here and followed by a discussion on the effects of wettability and the implication of the purging test.

2. Neutron radiography and image processing

Complimentary to X-ray, neutron imaging can penetrate metals but is attenuated by organic materials. Therefore neutron imaging is suitable for non-destructive inspection of mechanical devices. Its set up also allows for in situ experiments to be carried out as a series of 2D raw images, also called radiographs. The neutron attenuation coefficient of a material, which is its propensity to prevent neutrons from passing through, depends on its neutron cross-section and is independent of the atomic number which varies significantly with different isotopes. As shown in Fig. 2, the level of attenuation is much greater by water than aluminum.

In order to detect the thickness of water inside the cell the radiographs, shown in Fig. 3, require additional post-processing. Using a baseline image of a dry fuel cell, an image subtraction from a wet fuel cell image will result an image of only the water inside the cell. This principle is derived from the Lambert–Beer law which shows the relationship between the attenuation of the neutron and the thickness of a material:

$$I = I_0 e^{-\Sigma x}$$

where I_0 is the incident neutron flux and I is the transmitted neutron through the thickness, x , of a given medium with a probability per unit path length, Σ , that a neutron will interact as it moves about in a medium. With an image of a dry fuel cell, I_1 , and an image of a wet fuel cell, I_2 , given the material properties of the fuel cell and water, denoted with a subscript C and W , respectively, the resulting image can be expressed as

$$I_1 = I_0 e^{-[\Sigma_C x_C]}$$

$$I_2 = I_0 e^{-[\Sigma_C x_C + \Sigma_W x_W]}$$

After rearranging the terms, the subtraction operation follows as

$$[\Sigma_C x_C + \Sigma_W x_W] - \Sigma_C x_C = \Sigma_W x_W = -\ln\left(\frac{I_2}{I_0}\right) + \ln\left(\frac{I_1}{I_0}\right) = \ln\left(\frac{I_1}{I_2}\right)$$

The operation is partially automated in MATLAB using the *imdivide* command in the Image Processing Toolbox. In addition, a calibration block filled with a known thickness of water is also included in the images for estimating the thickness of water to correct for the power fluctuation of the nuclear reactor. A custom color map is used to render the post processed images to enhance the results.

3. Experimental setup

The experiments and imaging were performed at the McClellan Nuclear Radiation Center (MNRC), a facility operated by the University of California, Davis, in the facility’s Bay 3 beam line. The MNRC’s neutron beam has a thermal neutron flux rate of $4.6 \times 10^6 \text{ n cm}^{-2} \text{ s}^{-1}$ and a fast neutron flux rate of

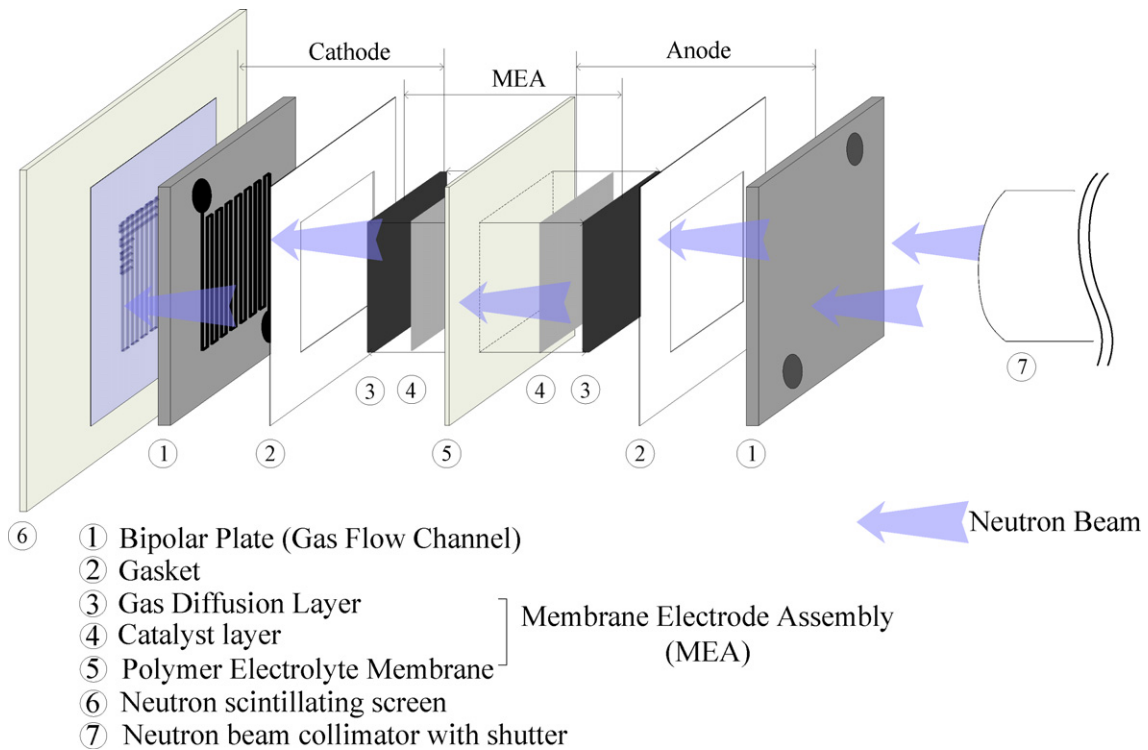


Fig. 1. In situ setup for neutron imaging of a fuel cell. The neutron beam penetrates the cell in the thickness direction. The image is captured by a CCD camera and post-process in MATLAB.

$2.2 \times 10^6 \text{ n cm}^{-2} \text{ s}^{-1}$ at the reactor's operation point of 1 MW. The beam aperture is 4 cm (1.54 in.) with an L/D ratio of 175. A $100 \mu\text{m}$ scintillation screen is used for light emission into the Apagee Alta camera, equipped with a $2048 \times 2048 \text{ } 13 \mu\text{m}$ pixel imaging array to capture the digital radiograph. The camera is fitted with a Nikon 105 mm $f/2.8$ lens at 25 s exposure times.

To maximize the contrast of the desired image, aluminum is used to construct the fuel cell mono-polar plates since it has a low neutron attenuation coefficient. However, there is a trade-off between cell performance due to the higher contact resistance with the oxide layer and the high neutron penetration to produce higher contrast images. A cell using untreated aluminum bipolar plates has a one-third the current density compared to a cell using nickel-coated aluminum bipolar plates. At the time of this work,

the super-hydrophobic and super-hydrophilic coatings were well developed for applying on aluminum, thus we decided to proceed with aluminum bipolar plates for the experiments. Two fuel cells were prepared, each with only the right-half of the flow field coated with either the super-hydrophilic or super-hydrophobic coating, leaving the left-half of the flow field untreated. Fig. 4 shows the schematic of the steps in the fabrication process. Prior to fabricating the bipolar plates, specimens were made with the same material to check the wetting characteristics. The contact angle was measured using the specimens, but not on the bipolar plates. To prepare the super-hydrophilic surface, the flow channels were sandblasted and anodized in a 0.3 M concentration of oxalic acid at 40 V and 25 °C over 12 h. This process increases the surface roughness of the aluminum making the plate super-hydrophilic.

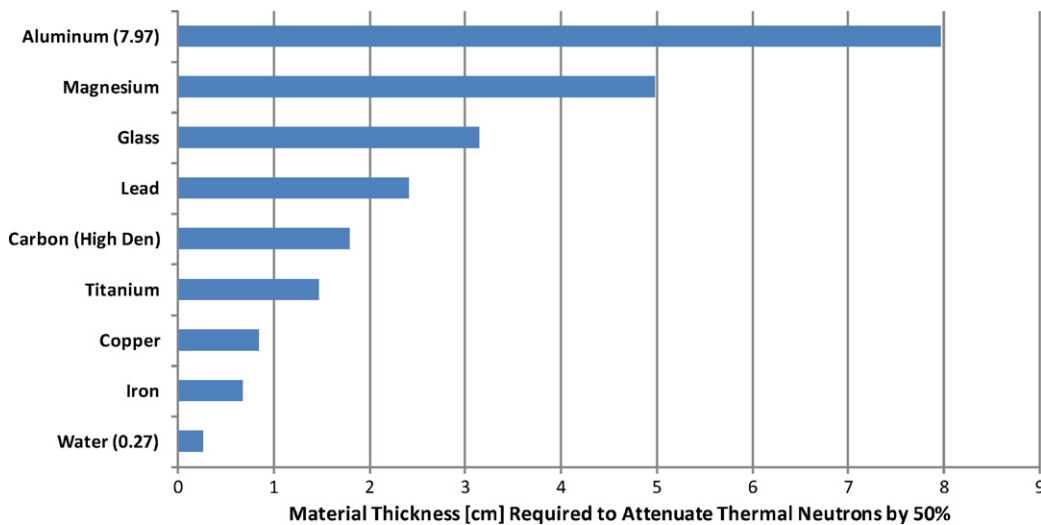


Fig. 2. Neutron attenuation of common materials. The x-axis shows the thickness required in cm to remove 50% of the thermal neutron from the beam. Noted that water has much higher attenuation than aluminum.

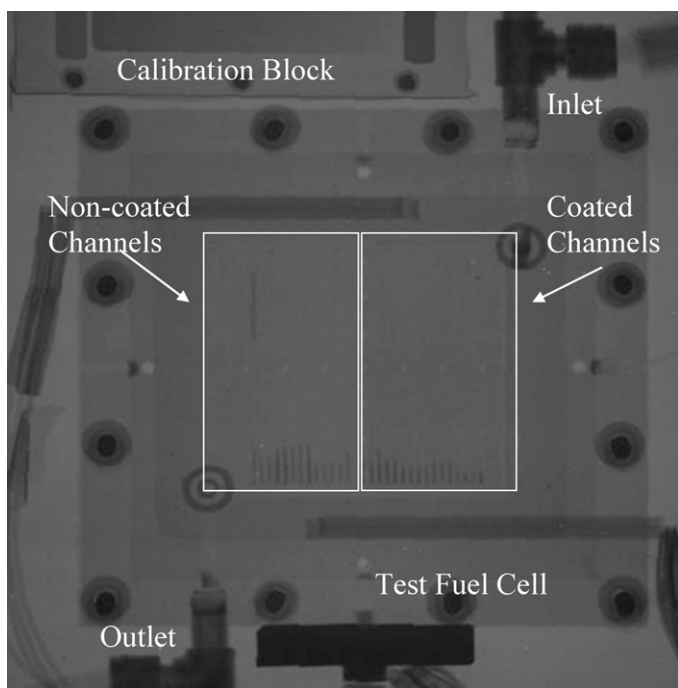
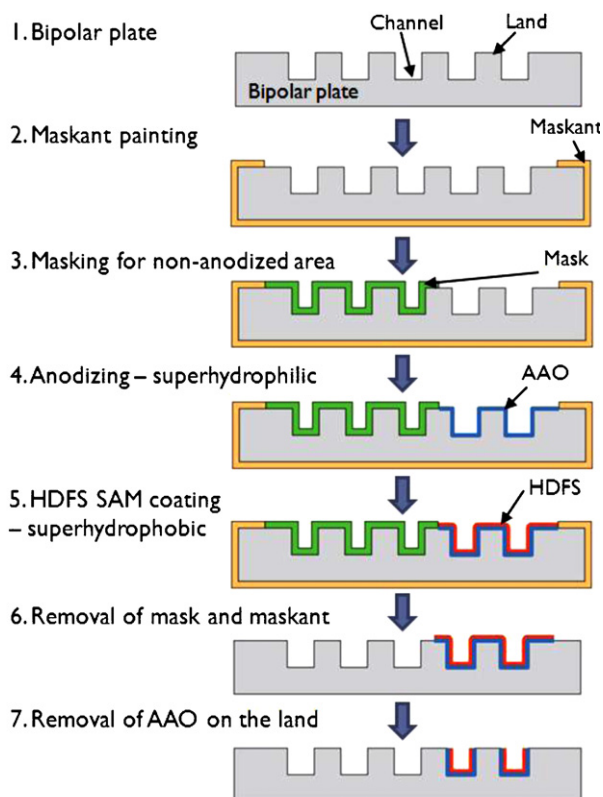


Fig. 3. Raw image captured by the CCD camera. The image includes a calibration block for measuring the water thickness inside the fuel cell and to calibrate for the fluctuation of the reactor power.

To achieve a super-hydrophobic coating, a self-assembled monolayer (SAM) was coated on the surface of flow channels using HDFS (heptadecafluoro-1,1,2,2-tetrahydrodecyl) trichlorosilane [43,44]. Finally, the aluminum oxide layer was removed along the top of the landing areas where the plates make contact with the GDL. Fig. 5 shows the SEM images of the hydrophilic bipolar plates after sand blasting to create micro-size roughness and anodization to create nano-size roughness respectively. Fig. 6 shows the behaviors of water on the bipolar plates with different wettability. The anode and cathode channels are 0.8 mm wide and 1 mm deep, as well as the header and footer channels connecting the parallel channels. The cells have a 48 cm² active area with 35 parallel flow channels forming the entire flow field. The inlets were purposely routed on the coated sides of the cells to prevent large slug formation which would block the exits, therefore creating dissimilar running conditions for the two cells. Furthermore, since the coatings on the landing area where the flow channels make contact with the GDL have been removed, the hydrophobicity of the individual channels should not have significant impact on the extraction of water from the GDL when the cell is at idle.



Notes:

Anodic Aluminum Oxide (AAO)

<(Heptadecafluoro-1,1,2,2-Tetrahydrodecyl) Trichlorosilane> (HDFS)

Maskant uses as mask

Fig. 4. Fabrication steps for producing the super-hydrophobic and super-hydrophilic coating on the bipolar plates.

The cell used a SGL 10BC carbon GDL and an Nafion 112 MEA with platinum loading of 0.4 mg cm⁻² on both sides. After the completion of a break-in cycle to hydrate the membrane, the fuel cell was brought to a wet initial condition before performing the purging experiment by running it at 0.3 V constant voltage for 20 min. This ensured both the MEA and GDL had sufficient water. External heaters were placed in the cell to maintain 80 °C operating temperature prior and during the purging to avoid the effects of condensation. The Arbin Fuel Cell Test Station (FCTS) was used to control the experiment which was programmed to supply fully humidified fuel and oxidant stream to the fuel cell. At 0.3 V constant voltage operation, the cell gave a 300 mA cm⁻² current density with

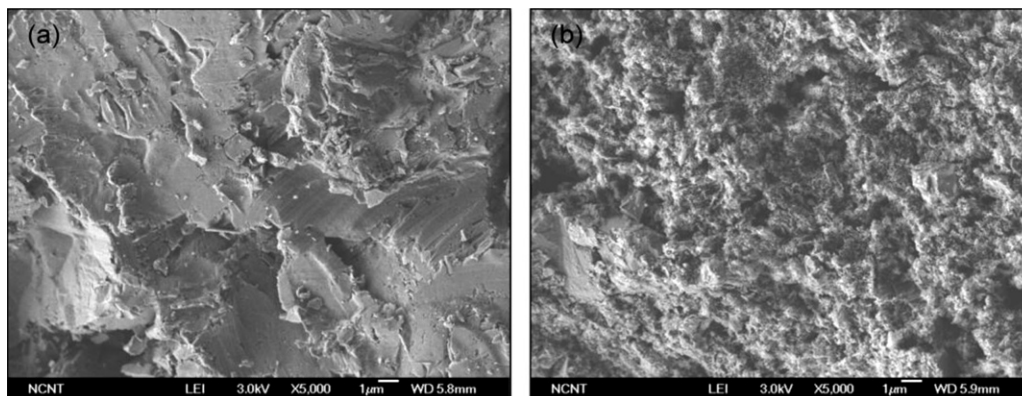


Fig. 5. SEM images of (a) surface after sand blasting, and (b) surface after sand blasting and anodization.

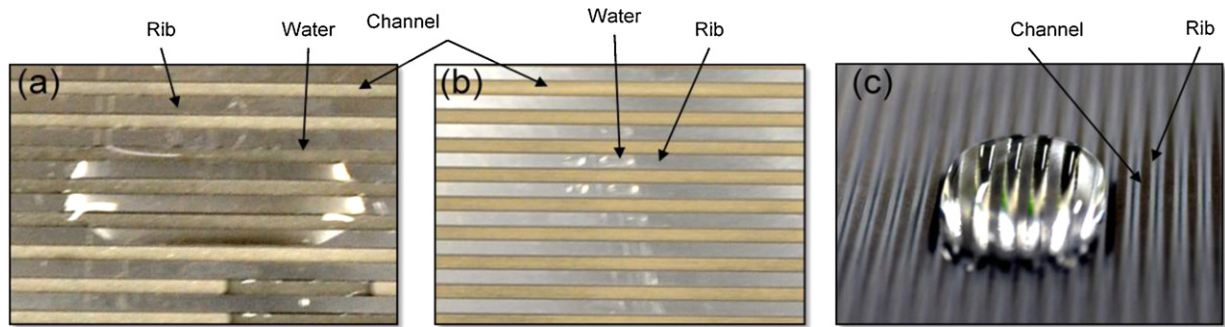


Fig. 6. Using water droplet to check wettability in channel: (a) hydrophilic surface – water adhere to channel and land, (b) super-hydrophilic surface – water spreads quickly in channel, and (c) super-hydrophobic surface – water cannot enter into channel.

the FCTS providing the minimum fuel flow rate at 80 sccm and oxidant flow rate at 160 sccm. The minimum flow rate is limited by the mass flow controller used and the resolution of the digital-to-analogue converter of the DSP used in the FCTS. This minimal flow rate gives an equivalent of 0.05 m s^{-1} gas flow rate in the fuel channel and 0.08 m s^{-1} in the oxidant channel. This flow rate is not sufficient to dry the water in the flow channel or from the GDL, and flooding is expected to occur. After the 20 min, all gas to the cell is shut-off.

An image was taken of the wet cell, its initial reference state, and then the cell was subjected to a sequence of six purge steps, 30 s each, with 20°C nitrogen at various flow velocities. The gas velocities used in these experiments were chosen from an analysis of related purge test studies [3,19,25,40,45,46]. Borrelli et al. [45] showed the removal of channel area water droplets from a superficial velocity of 0.7 m s^{-1} to 10 m s^{-1} in a single flow channel cathode mock cell. Though they gained insight into surface water removal, such optical methods using Lexan based plates have limited effectiveness on characterizing internal GDL water migration. Our test examines these studies' lower range of purge velocities spanning from 1 m s^{-1} to 4 m s^{-1} and analyzes the effectiveness of GDL water removal. The lower range was chosen due to the limitations of our system. After the purging stages, each cell was then dried thoroughly and a final dry image was taken for post processing purposes. The images were then post processed in MATLAB. The raw digital radiographs were first transformed into attenuation radiographs. The image of interest was then subtracted by the dry image to show the remaining water in the cell.

An estimation of water thickness throughout the flow-field was attained using calibration block attenuation data. The camera sensor is prone to noise during radiation exposure, which tends to be more detrimental to image quality in regions of lower signal intensity. Since the water content in these cells is relatively low resulting in weaker signals, noise was an initial concern. However, based on this data set, the attenuation profiles were very reasonable and consistent, containing minimal noise samples, so very little filtering was needed. One observation was that the landing areas, which have no coating, should have about the same amount of water trapped over them in both the super-hydrophobic and super-hydrophilic cells, at least initially. This trend was shown to be consistent and their amounts are graphed in Fig. 7. For the total mass calculation of the coatings, only the coated regions were accounted for in the MATLAB summing program.

4. Experimental results and discussion

Fig. 7 shows one set of images of the two fuel cells purged with nitrogen, specifically at 1 m s^{-1} and 4 m s^{-1} per channel. The non-coated/super-hydrophobic and non-coated/super-hydrophilic images at various purge gas velocities are shown

side-by-side for comparison. The difference in coatings may affect the flow conditions in the non-coated sections, therefore it is desirable to proceed comparing the coated to non-coated surface effects first and then examining the differences between the coated region's results. The larger manifolds of the cells reduced these effects by ensuring reasonably even flow distribution [47]. The following examines each scenario.

4.1. Super-hydrophilic/non-coated

These images show a progression of water removal as expected from a super-hydrophilic surface with a 1 m s^{-1} and 4 m s^{-1} purge gas velocity. In both the 1 m s^{-1} and 4 m s^{-1} wet cell, no large slugs are present on the super-hydrophilic side. This may be due to water forming a thin layer along the channel, rather than a slug, as a result of water trying to maximize its surface area. The non-coated side shows a different distribution with the presence of a large slug in the upper left portion of the flow field under the 1 m s^{-1} conditions, a factor that can lead to performance instability in larger stacks [48–50]. Though both sides show water build up at the channel exits a closer look shows the super-hydrophilic side to have a very even distribution of water content in each channel, under both velocity conditions. This water may be as a result of gravity induced collection, condensation and or GDL water rejection. The non-coated exit regions appear much more randomly distributed with some channels containing close to no water and others plugged more significantly. At 30 s in the 1 m s^{-1} run the slug has been removed and another has formed in the center of the non-coated side. The super-hydrophilic side water levels have dropped a bit and continue to do so over the course of the purge until at 120 s they are basically gone. In the case of the 4 m s^{-1} conditions water seems to be sufficiently removed at 60 s on the super-hydrophilic side. A noted difference of the non-coated sides is that during the slower velocity purge, water vacated the super-hydrophilic side channels several seconds before the non-coated side while at the higher velocity both sides were dried at a relatively equal rate, with the super-hydrophilic side actually maintaining traces of small scale water at the exits. In general the super-hydrophilic layer results in a thin coating of water along the channel walls, in which purge gas can easily bypass making it difficult to remove. The non-coated side water, in slug and droplet form, is more easily pushed out by purge gas. The hydrophilic layer in the flow channel, while maybe useful for preventing channel flooding during run conditions, is detrimental to cell purging.

4.2. Super-hydrophobic/non-coated

With the purge gas velocity from 1 m s^{-1} to 4 m s^{-1} on the super-hydrophobic surface, water droplets were easily pushed out of coated side channels because of the large contact angle between

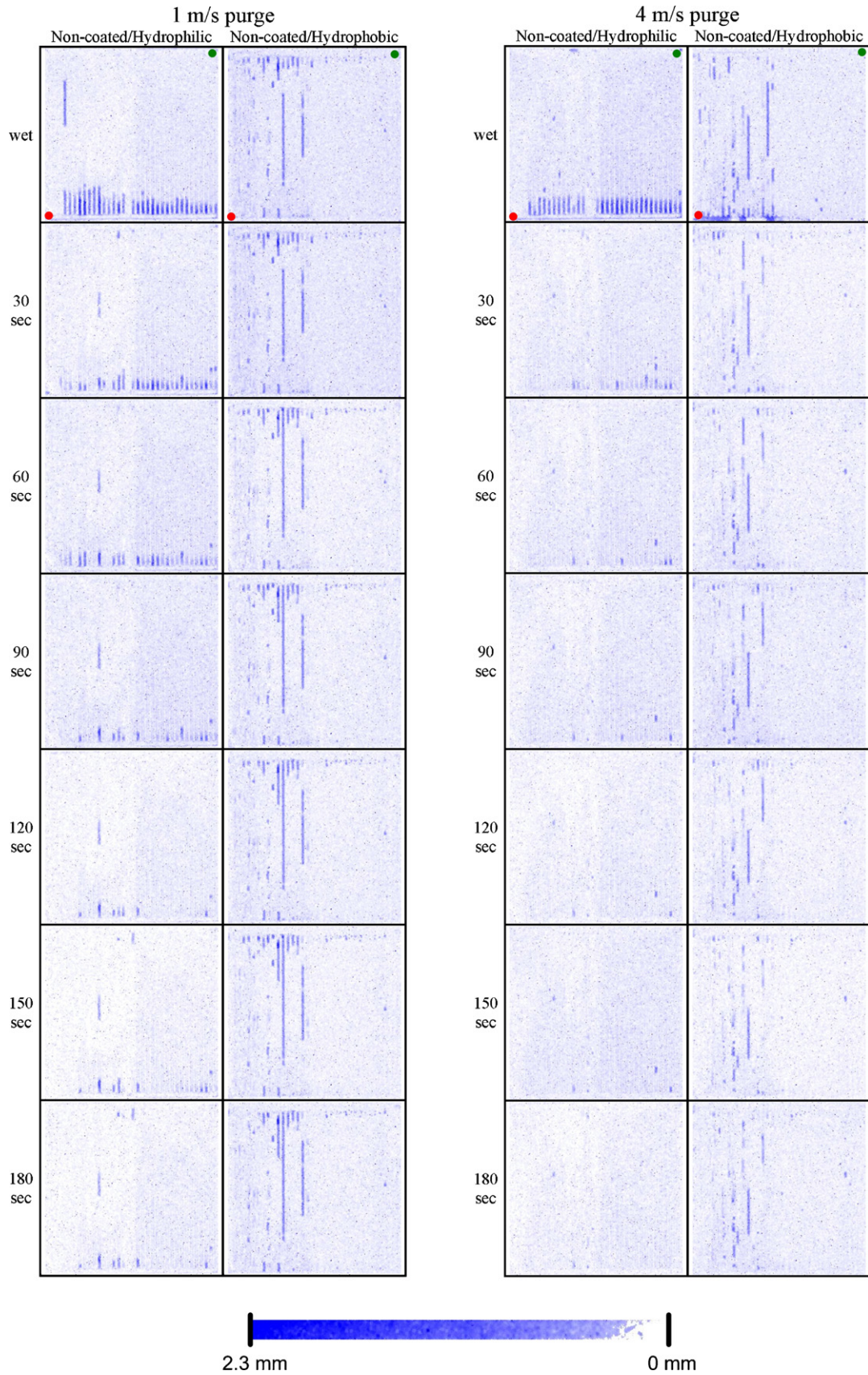


Fig. 7. The drying progress of the non-coated/hydrophobic and non-coated/hydrophilic flow channels. These images have been post-processed to enhance the visibility of the water remaining in the cell. Green dots indicate inlet while red indicates outlet. The color scale corresponds to the known water thickness taken from the post processing of the calibration block is shown on the bottom as reference. (For interpretation of the references to color in this figure legend, the reader is referred to the web version of the article.)

the droplet and the channel wall. Smaller droplets forming on the super-hydrophobic channel surface have an increased mobility in the cell and are easily guided out by gas flow. In addition to the moving gas, gravity may have also contributed to removing the water in the coated channels. The result of these combined phenomena left close to no water in the super-hydrophobic cell channel areas prior to the purge. Regarding the previously discussed effects that the coated side design has on the non-coated side design; large slugs seen plugging the non-coated side may be a result of the purge gas bypassing the plugged non-coated channels and flowing through the unobstructed super-hydrophobic channels. Slugs in the non-coated channels are difficult to purge under all velocity conditions, while the purging of the super-hydrophobic channels is very effective. The extent of slug formation in the non-coated channels indicates that hydrogen and air gas velocities from 1 m s^{-1} to 4 m s^{-1} were insufficient to compensate entirely for these coating effects completely. The progression of the purging process shows the rate of which the water is removed from the cell is similar in all velocity conditions. Further evidence can be found by computing the mass of water inside the cell, which will be described in the next section.

4.3. Super-hydrophobic/super-hydrophilic mass calculation

Fig. 8 shows a schematic which describes how both super-hydrophobic and super-hydrophilic coated channels tend to behave during purging. Water droplets formed in the non-coated channels adhered to the walls and blocked the gas flow. This is evident in the images after 120 s of purge for the non-coated sides, where water slugs remained in the channels under all velocity conditions. On the other hand, the super-hydrophobic coated channels cause droplets to bead and shed off the wall quickly, which is advantageous for preventing flooding. The super-hydrophilic coated channels reform the droplets into a film along the walls allowing gas to flow past, though now through a reduced cross sectional area. To best compare the two, we have estimated the amount of water in the cell by correlating the attenuation level to the known water thickness to attain a summation of the water mass.

Graphs in Figs. 9 and 10 show water amounts in the flow channels and over the landings, respectively. The general trends discussed in the literature [51–53], relating increased purge times

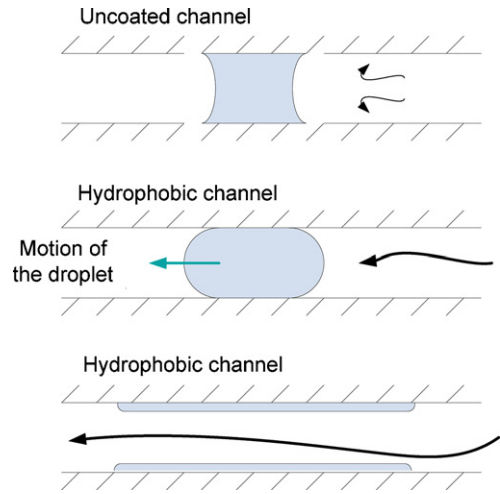


Fig. 8. The behavior of water droplet in the three types of channels in the experiments.

and higher velocities to increased water removal, were validated by our results. It was important to keep the running conditions and exposure time of the cell consistent in the experiment to show the overall cell behavior, the results reported here are from a single trial without averaging. The test cell was pre-run with the same procedure in order to achieve a similar initial condition. The initial water content could dramatically impact the results, but the general trend and effect of the purging gas velocity were preserved in the experiment. The dynamics of the water removal were different during the various stages of the experiment. For example, in the first few seconds of the purging, the water slugs were pushed out by the purging gas. Then, the remaining water was removed via diffusion, evaporation, and or dragging of droplets due to fluid friction from the moving gas. Regarding each cell's initial conditions just prior to purge, the super-hydrophilic cell contained more water than the super-hydrophobic cell. This agrees with our predictions, since super-hydrophilic surfaces tend to hold water better. At high purge gas velocity, the amount of water decreased significantly during the first 30 s. At low purge gas velocity, the slower rate of water removal may indicate the water was extracted by the dry gas rather than being pushed out. It is difficult to judge from the

Water over Lands at Various Purge Gas Speed

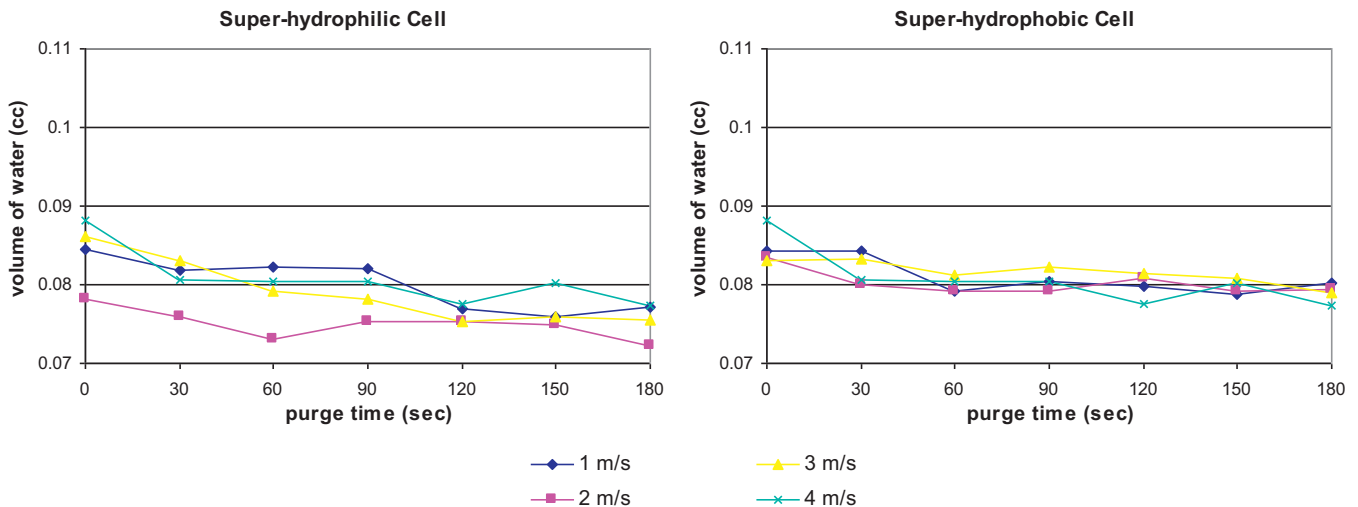


Fig. 9. Both cells show the amount of water in the flow channels decreases over time. The data suggest both hydrophilic and hydrophobic coatings have similar performance on improving the removal of water in the channels.

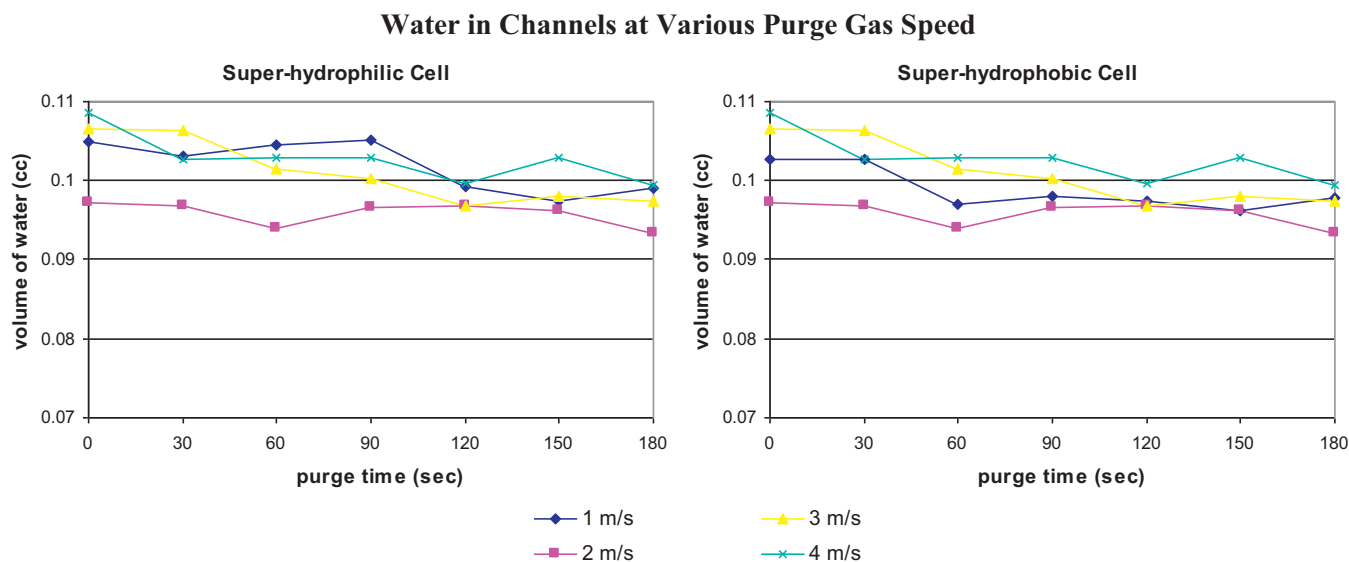


Fig. 10. The hydrophilic coating has better improvement over the hydrophobic cell in removing water from the landings. Although the coatings were removed on the landings where they contact with the GDL, the coatings in the channels may be helping to remove the water as it is pushed out by the purging gas.

mass data only if the super-hydrophobic or super-hydrophilic coating is clearly improving the water removal in the channels because the amount of water initially in the cell may be obscuring the results after 30 and 60 s into the purging, and they achieve compatible results after 180 s. However, also taking into account the water over the landings suggests the super-hydrophilic coating is improving the water removal. This may be because as the purge gas draws the water away from the land into the channel, the super-hydrophilic channels help to pull the water out from the GDL. Qualitatively, the purge gas velocities at 3 m s^{-1} and 4 m s^{-1} have about the same results. Table 2 summarizes the results we mentioned above.

There is another important implication to these results. Assuming the ideal purge gas velocity is 3 m s^{-1} for 60 s, it requires approximately 600 L h^{-1} gas flow rate for the cells in the experiment. This may require additional equipment or a purge gas system in order to properly dry the cell. This may be difficult or infeasible in many applications including mobile and transportation usage. In visualizing the non-coated/super-hydrophobic cell, it would appear that the cell has inferior performance. This may indicate that high resistance in the flow channel due to blockage is a more severe problem. While the super-hydrophilic coating does hold onto a thin layer of water during purging, it helps to thin out the water thus opening the channel for the purge gas. On the other hand, the super-hydrophobic coating helps to break up large droplets in the channel improving the water removal from the channels. Both seem to be favorable for removing water in the channel by purging, however, further consideration is needed, for example high current density

or recycling water from the cathode to the anode by pressure differences, when choosing the appropriate coating method.

5. Conclusion

With water in the flow channels potentially creating problems during start-up/shutdown and operation in cold environment, it is necessary to purge the PEM fuel cell to remove the water from the channels. We investigated the benefit of the super-hydrophobic and super-hydrophilic surface modification on the flow channels for removing water by purging with nitrogen gas, and found that while the super-hydrophobic coating helps to keep the water content low in the channels and improve the purging of the water out from the channels, the super-hydrophilic coating helps to pull water out of the landings area. Although both surface modification method seem to improve the water removal over the non-coated channels, further consideration is needed to choose the favorable solution.

Further studies are needed to investigate the benefit of the surface modification for larger flow field, and the performance stability in a stack configuration. Much near term studies are the effects of orientation and gravity in selecting the appropriate coating methods, and the combine use of super-hydrophilic coating on the anode side and super-hydrophobic coating on the cathode side to improve the water migration through the MEA by concentration.

Acknowledgements

The authors wish to acknowledge the researchers at McClellan Nuclear Radiation Center: Ronald Walker, Harold Egbert, and Hungyuan Liu, for their support and access to the facility. This work was supported by the National Research Foundation of Korea (NRF) grant funded by the Korea government (MEST) (No. 2010-0018457).

References

- [1] Risø Energy Report 3 – Hydrogen and its competitors, Technical University of Denmark, Risø National Laboratory for Sustainable Energy, Frederiksborgvej 87-550-3350-4, October 2004.
- [2] S.-J. Lim, G.-G. Park, J.-S. Park, Y.-J. Sohn, S.-D. Yim, T.-H. Yang, B.K. Hong, C.-S. Kim, International Journal of Hydrogen Energy 35, pp.13111–13117.

Table 2
Comparison of the performance of water removal on different surface conditions.

	Low current density operation ^a	Purging	
		Over landings	In channels
Hydrophilic	○ ^b	+	○ ^c
Hydrophobic	+	–	+
Non-coated	–	○	–

^a The results refers to the data at the unpurged condition, which is representative to the condition during the operation of the cell.

^b The coating did not dramatically cause flooding during the experiments.

^c It is difficult to purge the thin film of water on the wall, but water does not form slugs.

- [3] J.P. Owejan, J.J. Gagliardo, J.M. Sergi, S.G. Kandlikar, T.A. Trabold, *International Journal of Hydrogen Energy* 34 (2009) 3436–3444.
- [4] R. Schweiss, M. Steeb, P.M. Wilde, *Mitigation of Water Management in PEM Fuel Cell Cathodes by Hydrophilic Wicking Microporous Layers*, vol. 10, Wiley-VCH Verlag, pp. 1176–1180.
- [5] J. Wu, X.Z. Yuan, J.J. Martin, H. Wang, J. Zhang, J. Shen, S. Wu, W. Merida, *Journal of Power Sources* 184 (2008) 104–119.
- [6] C.R. Buie, J.D. Posner, T. Fabian, S.-W. Cha, D. Kim, F.B. Prinz, J.K. Eaton, J.G. Santiago, *Journal of Power Sources* 161 (2006) 191–202.
- [7] D.P. Wilkinson, H.H. Voss, K. Prater, *Journal of Power Sources* 49 (1994) 117–127.
- [8] D.M. Bernardi, M.W. Verbrugge, *Journal of the Electrochemical Society* 139 (1992) 2477–2491.
- [9] H.H. Voss, D.P. Wilkinson, P.G. Pickup, M.C. Johnson, V. Basura, *Electrochimica Acta* 40 (1995) 321–328.
- [10] L. Cindrella, A.M. Kannan, J.F. Lin, K. Saminathan, Y. Ho, C.W. Lin, J. Wertz, *Journal of Power Sources* 194 (2008) 146–160.
- [11] T. Fabian, R. O'Hayre, S. Litster, F.B. Prinz, J.G. Santiago, *Journal of Power Sources* 195 (10) (2010) 3201–3206.
- [12] U. Pasaogullari, C.-Y. Wang, *Journal of the Electrochemical Society* 152 (2005) A380–A390.
- [13] M.W. Knobbe, W. He, P.Y. Chong, T.V. Nguyen, *Journal of Power Sources* 138 (2004) 94–100.
- [14] A. Taniguchi, K. Yasuda, *Journal of Power Sources* 141 (2005) 8–12.
- [15] T. Metz, N. Paust, C. Müller, R. Zengerle, P. Koltay, *Sensors and Actuators A: Physical* 143 (2008) 49–57.
- [16] J. Chen, T. Matsuura, M. Hori, *Journal of Power Sources* 131 (2004) 155–161.
- [17] J.W. Choi, Y.-S. Hwang, J.-H. Seo, D.H. Lee, S.W. Cha, M.S. Kim, *International Journal of Hydrogen Energy* 35 (8) (2010) 3698–3711.
- [18] T. Fabian, R. O'Hayre, S. Litster, F.B. Prinz, J.G. Santiago, *Journal of Power Sources* 195 (11) (2010) 3640–3644.
- [19] K. Tajiri, C.-Y. Wang, Y. Tabuchi, *Electrochimica Acta* 53 (2008) 6337–6343.
- [20] T. Van Nguyen, M.W. Knobbe, *Journal of Power Sources* 114 (2003) 70–79.
- [21] J.S. Yi, J.D. Yang, C. King, *Water Management Along the Flow Channels of PEM Fuel Cells* 50, American Institute of Chemical Engineers, 2004, pp. 2594–2603.
- [22] J. Zhang, Z. Qi, *PEM Fuel Cell Electrocatalysts and Catalyst Layers*, Springer, London, 2008, pp. 547–607.
- [23] A. Turhan, S. Kim, M. Hatzell, M.M. Mench, *Electrochimica Acta* 55 (8) (2010) 2734–2745.
- [24] P.J. Hamilton, B.G. Pollet, *Polymer Electrolyte Membrane Fuel Cell (PEMFC) Flow Field Plate: Design, Materials and Characterisation* 10: Wiley-VCH Verlag, pp. 489–509.
- [25] X.G. Yang, F.Y. Zhang, A.L. Lubawy, C.Y. Wang, *Electrochemical and Solid-State Letters* 7 (2004) A408–A411.
- [26] J. Wu, X.Z. Yuan, H. Wang, M. Blanco, J.J. Martin, J. Zhang, *International Journal of Hydrogen Energy* 33 (2008) 1735–1746.
- [27] J. Wu, X. Zi Yuan, H. Wang, M. Blanco, J.J. Martin, J. Zhang, *International Journal of Hydrogen Energy* 33 (2008) 1747–1757.
- [28] R.C. McDonald, C.K. Mittelsteadt, E.L. Thompson, *Effects of Deep Temperature Cycling on Nafion® 112 Membranes and Membrane Electrode Assemblies*, *Fuel Cells* 4 (3) (2004) 208–213, Wiley-VCH Verlag.
- [29] Z. Zhan, C. Wang, W. Fu, M. Pan, *International Journal of Hydrogen Energy*, doi:10.1016/j.ijhydene.2011.02.081, in press (corrected proof).
- [30] D. Spornjak, A.K. Prasad, S.G. Advani, *Journal of Power Sources* 170 (2007) 334–344.
- [31] A. Esposito, A.D. Montello, Y.G. Guezennec, C. Pianese, *Journal of Power Sources* 195 (9) (2010) 2691–2699.
- [32] A. Esposito, A.D. Montello, Y.G. Guezennec, C. Pianese, *Journal of Power Sources* 195 (11) (2010) 3365–3373.
- [33] S. Litster, D. Sinton, N. Djilali, *Journal of Power Sources* 154 (2006) 95–105.
- [34] S.-J. Lee, S.-G. Kim, G.-G. Park, C.-S. Kim, *International Journal of Hydrogen Energy* 35 (19) (2010) 10457–10463.
- [35] K. Takada, Y. Ishigami, J. Inukai, Y. Nagumo, H. Takano, H. Nishide, M. Watanabe, *Journal of Power Sources* 196, 2635–2639.
- [36] H. Murakawa, T. Ueda, K. Sugimoto, H. Asano, N. Takenaka, *Nuclear Instruments and Methods in Physics Research Section A: Accelerators, Spectrometers, Detectors and Associated Equipment* (2010), doi:10.1016/j.nima.2010.12.046, in press (corrected proof).
- [37] N. Takenaka, H. Asano, K. Sugimoto, H. Murakawa, N. Hashimoto, N. Shindo, K. Mochiki, R. Yasuda, *Nuclear Instruments and Methods in Physics Research Section A: Accelerators, Spectrometers, Detectors and Associated Equipment* (2011), doi:10.1016/j.nima.2011.01.003, in press (corrected proof).
- [38] Y.H. Cai, J. Hu, H.P. Ma, B.L. Yi, H.M. Zhang, *Journal of Power Sources* 161 (2006) 843–848.
- [39] B. Mondal, K. Jiao, X. Li, *Three-Dimensional Simulation of Water Droplet Movement in PEM Fuel Cell Flow Channels with Hydrophilic Surfaces*, John Wiley & Sons, Ltd, 2011.
- [40] K. Tüber, D. Pócza, C. Hebling, *Journal of Power Sources* 124 (2003) 403–414.
- [41] E.C. Kumbur, K.V. Sharp, M.M. Mench, *Journal of Power Sources* 161 (2006) 333–345.
- [42] J. Park, X. Li, *Journal of Power Sources* 163 (2007) 853–863.
- [43] Y. Ohkubo, I. Tsuji, S. Onishi, K. Ogawa, *Journal of Materials Science* 45, pp. 4963–4969.
- [44] K.-Y. Yang, J.-W. Kim, K.-J. Byeon, H. Lee, *Microelectronic Engineering* 84 (2007) 1552–1555.
- [45] J. Borrelli, S.G. Kandlikar, T. Trabold, J. Owejan, *Evolution* 2005 (2005) 625–633.
- [46] S. Ge, C.-Y. Wang, *Journal of The Electrochemical Society* 154 (2007) B998–B1005.
- [47] S. Maharudrayya, S. Jayanti, A.P. Deshpande, *Journal of Power Sources* 144 (2005) 94–106.
- [48] P.A.C. Chang, J. St-Pierre, J. Stumper, B. Wetton, *Journal of Power Sources* 162 (2006) 340–355.
- [49] M. Miller, A. Bazylak, *Journal of Power Sources* 196 (2) (2011) 601–613.
- [50] G. Squadrito, O. Barbera, G. Giacoppo, F. Urbani, E. Passalacqua, *International Journal of Hydrogen Energy* 33 (2008) 1941–1946.
- [51] *Optimizing fuel cell water purge cycles*, *Fuel Cells Bulletin* 4 (2001) 16.
- [52] *System and method for optimizing fuel cell stack purge cycles*, *Fuel Cells Bulletin* 4 (2001) 15.
- [53] X. Yu, M. Pingwen, H. Ming, Y. Baolian, Z.-G. Shao, *Journal of Power Sources* 188 (2009) 163–169.